



Cite this: *Phys. Chem. Chem. Phys.*, 2022, 24, 3918

La@[La₅⊕B₃₀]^{0/-/2-}: endohedral trihedral metallo-borosphenes with spherical aromaticity†

Mei-Zhen Ao,^{ab} Xiao-Qin Lu,^a Yue-Wen Mu,^{id}*^a Wen-Yan Zan^{id}*^a and Si-Dian Li^{id}*^a

It is well-known that transition-metal-doping induces dramatic changes in the structures and bonding of small boron clusters, as demonstrated by the newly observed perfect inverse sandwich D_{8h} [La(η^8 -B₈)La] and D_{9h} [La(η^9 -B₉)La]⁻. Based on extensive global minimum searches and first-principles theory calculations, we predict herein the possibility of perfect endohedral trihedral metallo-borosphenes D_{3h} La@[La₅⊕B₃₀] (**1**, ³A₁) and its monoanion C_s La@[La₅⊕B₃₀]⁻ (**2**, ²A') and dianion D_{3h} La@[La₅⊕B₃₀]²⁻ (**3**, ¹A₁). These La-doped boron clusters are composed of three inverse sandwich La(η^8 -B₈)La on the waist and two inverse sandwich La(η^9 -B₉)La on the top and bottom which share one apex La atom at the center and six periphery B₂ units between neighboring η^8 -B₈ and η^9 -B₉ rings, with three octo-coordinate La atoms and two nona-coordinate La atoms as integrated parts of the cage surface. Detailed adaptive natural density partitioning (AdNDP) and iso-chemical shielding surface (ICSS) analyses indicate that La@[La₅⊕B₃₀]^{0/-/2-} (**1/2/3**) are spherically aromatic in nature. The one-dimensional nanowire La₄B₂₁ (**4**, $P\bar{3}1m$) constructed from D_{3h} La@[La₅⊕B₃₀] (**1**) along the C₃ axis of the system appears to be metallic. The IR and Raman spectra of La@[La₅⊕B₃₀] (**1**) and photoelectron spectroscopy of the slightly distorted C_s La@[La₅⊕B₃₀]⁻ (**2**) are theoretically simulated to facilitate their spectroscopic characterizations.

Received 10th December 2021,
 Accepted 24th January 2022

DOI: 10.1039/d1cp05644a

rsc.li/pccp

Introduction

Due to its prototypic electron deficiency, boron tends to form delocalized multicenter-two-electron (mc-2e) bonds in both its polyhedral molecules and bulk allotropes, resulting in a great structural diversity in boron nanostructures.^{1,2} Persistent joint photoelectron (PE) spectroscopy and first-principles theory investigations by Wang and co-workers in the past two decades have unveiled a rich landscape for B_{*n*}^{-/0} boron clusters from planar or quasi-planar structures (2D) ($n = 3-38, 41, 42$), seashell-like B₂₈^{-/0}, cage-like borosphenes B₄₀^{-/0} and B₃₉⁻, to bilayer B₄₈^{-/0, 3-8}. The newly discovered bilayer motif has been recently extended to a large size range of even numbered neutral boron clusters between B₄₈-B₇₂ at density functional theory (DFT) level.⁹⁻¹¹ Ion mobility and theoretical calculations, on the other hand, showed that B_{*n*}⁺ monocations possess tubular structures in the size range $n = 16-25$.¹² Perfect cage-like B₈₀ has also been proposed at density functional theory

(DFT)^{13,14} level which was later found to favor core-shell structures in thermodynamics.¹⁵

Extensive experimental and theoretical investigations indicate that transition-metal-doping induces dramatic changes in the structures and bonding of boron nanoclusters. The close-packed quasi-planar C_s B₁₀⁻ was transformed into perfect monocyclic wheel structures in both D_{10d} Ta@B₁₀⁻ and D_{10d} Nb@B₁₀⁻,¹⁶ while the Co-centered D_{8d}/C_{4v} CoB₁₆⁻ adopted double-ring tubular drum-like structures.¹⁷ A series of di-La-doped perfect inverse sandwich complexes D_{7h} [La(η^7 -B₇)La]⁻, D_{8h} [La(η^8 -B₈)La], and D_{9h} [La(η^9 -B₉)La]⁻ were observed in combined PES and theoretical investigations,^{18,19} while tri-La-doped La₃B₁₄⁻ was found to possess an inverse triple-decker La-B₈-La-B₈-La geometry.²⁰ The first experimentally observed spherical trihedral metallo-borosphenes La₃B₁₈⁻ with three equivalent deco-coordinate La atoms as integral parts of the cage surface²¹ was late extended to the smallest core-shell-like metallo-borosphenes D_{3h} La₃B₂₀⁻ (La₃&[B₂@B₁₈]⁻) at first-principles theory level.²² The smallest metallo-borosphenes D_{3h} Ta₃B₁₂⁻ with three equivalent octa-coordinate Ta centers in three η^8 -B₈ rings and spherical aromatic T_d Ta₄B₁₈ with four equivalent nona-coordinate Ta centers in four η^9 -B₉ rings were late predicted in theory.^{23,24} Endohedral metallo-borosphenes D_2 Ta@B₂₂⁻ was also predicted to be a superatom matching the 18-electron rule.²⁵ The experimentally observed organometallic

^a Nanocluster Laboratory, Institute of Molecular Science, Shanxi University, Taiyuan 030006, P. R. China

^b Fenyang College of Shanxi Medical University, Fenyang 032200, China.
 E-mail: ywmu@sxu.edu.cn, zanwy@sxu.edu.cn, lisidian@sxu.edu.cn

† Electronic supplementary information (ESI) available. See DOI: 10.1039/d1cp05644a

complexes $T_d \text{An}@C_{28}$ ($\text{An} = \text{Th}, \text{Pa}^+, \text{U}^{2+}, \text{Pu}^{4+}$) were found to be superatoms following 32-electron principle.²⁶ Highly stable endohedral metallo-borospherenes $O_h \text{La}_6\&[\text{La}@B_{24}]^{+/0}$ have been predicted to be embryos of low-dimensional lanthanide boride nanomaterials.²⁷ However, whether larger endohedral metallo-borospherenes with spherical aromaticity exist or not and if such clusters can be used as building blocks to form low-dimensional boron nanomaterials still remain unknown to date in both theory and experiments.

Keeping inspirations from the experimentally observed inverse sandwiches $D_{8h} [\text{La}(\eta^8\text{-B}_8)\text{La}]$ and $D_{9h} [\text{La}(\eta^9\text{-B}_9)\text{La}]^-$ in mind and based on extensive first-principles theory calculations, we predict herein the perfect endohedral trihedral metello-borospherene $D_{3h} \text{La}@[\text{La}_5\&\text{B}_{30}]$ (**1**, $^3A'_1$) and its monoanion $C_s \text{La}@[\text{La}_5\&\text{B}_{30}]^-$ (**2**, $^2A'$) and dianion $D_{3h} \text{La}@[\text{La}_5\&\text{B}_{30}]^{2-}$ (**3**, $^1A'_1$) which turn out to be spherically aromatic in nature. Using $\text{La}@[\text{La}_5\&\text{B}_{30}]$ (**1**) as building blocks, the metallic one-dimensional (1D) nanowire La_4B_{21} ($P31m$) (**4**) can be achieved as an extension of the system along the C_3 axis.

Theoretical methods

Extensive global minimum (GM) searches were performed on La_6B_{30} using the TGMIn 2.0 package,^{28,29} in combination with manual structural constructions. More than 3800 stationary points in different spin multiplicities on the potential energy surface were probed at PBE0/TZVP level. The thirty lowest-lying isomers of La_6B_{30} were fully optimized at the hybrid PBE0³⁰ and TPSSH³¹ level with the 6-311 + G* basis set³² for B and Stuttgart energy-consistent pseudopotential ECP46MWB with the corresponding ECP46MWB basis set^{33,34} for La, with harmonic vibrational frequencies checked to make all the obtained isomers are true minima of the systems. Low-lying isomers of the monoanion $\text{La}_6\text{B}_{30}^-$ and dianion $\text{La}_6\text{B}_{30}^{2-}$ were obtained from the corresponding low-lying structures of neutral La_6B_{30} , with additional global searches executed to locate the true GMs of the anions. Geometrical optimizations and vibrational frequency checks were implemented with the Gaussian 09 program.³⁵ Single-point calculations at the more accurate CCSD(T) level^{36,37} were performed employing Molpro program³⁸ at PBE0 geometries with the basis set of 6-31G(d) for B and the Stuttgart pseudopotential ECP46MWB for La. Natural bonding orbital (NBO) analyses were performed using the NBO 6.0 program³⁹ and detailed bonding analyses carried out utilizing the adaptive natural density partitioning (AdNDP) approach.^{40,41} Born–Oppenheimer molecular dynamic (BOMD) simulation was implemented employing the CP2K code⁴² with the GTH-PBE pseudopotential and the TZVP-MOLOPT-SR-GTH basis set. Iso-chemical shielding surfaces (ICSSs) were generated with the Multiwfn 3.7 code.⁴³ The visualization for the isosurfaces of various functions has been realized with VMD software.⁴⁴ The PE spectrum $\text{La}_6\text{B}_{30}^-$ was simulated using the time-dependent TD-DFT-PBE0 approach⁴⁵ which has been successfully used in various boron-based monoanion clusters.^{3–8,16–22}

Calculations on 1D La_4B_{21} (**4**) nanowire were performed using the Vienna *ab initio* simulation package (VASP),^{46,47} within the framework of projector augmented wave (PAW) pseudopotential method^{48,49} and PBE generalized gradient approximation (GGA).^{50,51} The Coulomb-corrected local spin-density approximation (LSDA+ U) was utilized for both structural optimizations and static calculation ($U = 5$ eV).^{52,53} The energy cutoff for plane-wave basis set was set to 450 eV. Atomic structures are fully relaxed using the conjugate gradient method until the maximum force on each atom was less than 0.01 eV \AA^{-1} and the energy precision was set to 10^{-5} eV. The phonon spectrum was calculated using the density functional perturbation theory (DFPT) method with the Phonopy code combined with VASP package at the PBE level.⁵⁴

Results and discussion

Structures and stability

Thus obtained lowest-lying structures of $D_{3h} \text{La}@[\text{La}_5\&\text{B}_{30}]$ (**1**, $^3A'_1$), $C_s \text{La}@[\text{La}_5\&\text{B}_{30}]^-$ (**2**, $^2A'$), and $D_{3h} \text{La}@[\text{La}_5\&\text{B}_{30}]^{2-}$ (**3**, $^1A'_1$) are depicted in Fig. 1, with more alternative low-lying isomers tabulated in Fig. S1–S3 (ESI[†]). The lowest-lying triplet $\text{La}@[\text{La}_5\&\text{B}_{30}]$ (**1**) with the smallest vibrational frequency of 109.5 cm^{-1} possesses a perfect D_{3h} trihedral spherical structure with two degenerate singly occupied molecular orbitals (SOMOs, e') according to Hund's rule (Fig. S4, ESI[†]). It has two slightly distorted closed-shell neutral isomers $C_s \text{La}_6\text{B}_{30}$ (**NE-2**, $^1A'$) and $C_1 \text{La}_6\text{B}_{30}$ (**NE-3**, 1A) which appear to be only 0.01 eV and 0.02 eV less stable than $D_{3h} \text{La}@[\text{La}_5\&\text{B}_{30}]$ (**1**, $^3A'_1$) at CCSD(T) level, respectively (Fig. S1, ESI[†]), well supporting the relative energy orders obtained at both PBE0 and TPSSH. These close-lying isomers are practically iso-energetic in thermodynamics and may co-exist and compete in gas-phase experiments. Fig. S5 (ESI[†]) shows the variation of the relative Gibbs free energies for the lowest-lying four isomers of $\text{La}@[\text{La}_5\&\text{B}_{30}]$ as a function of temperature, further indicating that the three lowest-lying isomers (**NE-1**, **NE-2**, and **NE-3**) have minor differences in Gibbs free energies and may coexist experimentally. As collectively shown in Fig. S1 (ESI[†]), the twenty-five lowest-lying isomers of La_6B_{30} (**NE-1–NE-25**) within 1.80 eV all possess endohedral metallo-borospherene structures, with the first quintet isomer $C_s \text{La}@[\text{La}_5\&\text{B}_{30}]$ ($^5A'$) (**NE-8**) being much less

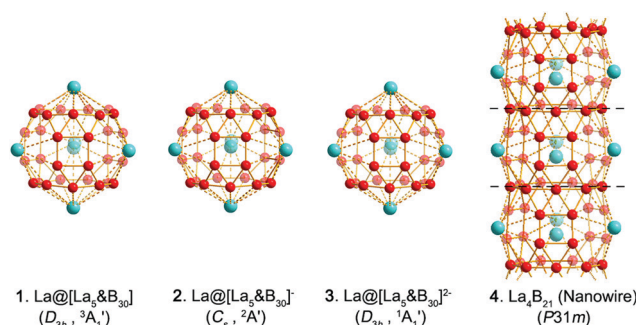


Fig. 1 Optimized structures of $\text{La}@[\text{La}_5\&\text{B}_{30}]$ (**1**), $\text{La}@[\text{La}_5\&\text{B}_{30}]^-$ (**2**), $\text{La}@[\text{La}_5\&\text{B}_{30}]^{2-}$ (**3**) and one-dimensional La_4B_{21} nanowire (**4**).

stable than D_{3h} GM (1) by 1.06 eV at PBE0. The much concerned core-shell isomers with a B_2 (NE-28), B_3 (NE-29 and Ne-30), or B_4 (NE-27) core at the center are found to lie at least 3.66 eV above the D_{3h} GM at PBE0. Attachment of one extra electron to D_{3h} $\text{La}@[La_5\&B_{30}]$ (1) generates its doublet monoanion of C_s $\text{La}@[La_5\&B_{30}]^-$ (2, $^2A_1'$) which is slightly distorted due to Jahn-Teller effect. Attachment of two extra electrons in the two singly occupied SOMOs (e') of D_{3h} $\text{La}@[La_5\&B_{30}]$ (1) results in the perfect singlet dianion D_{3h} $\text{La}@[La_5\&B_{30}]^{2-}$ (3, $^1A_1'$) (Fig. 1 and Fig. S4, ESI†). As clearly shown in Fig. S6 and S7 (ESI†), both monoanion $\text{La}@[La_5\&B_{30}]^-$ (2) and dianion $\text{La}@[La_5\&B_{30}]^{2-}$ (3) are the well-defined GMs of the systems which lie at least 0.6 eV lower in Gibbs free energies than their corresponding second lowest-lying isomers C_s $\text{La}_6\text{B}_{30}^-$ (MA-2) and C_s $\text{La}_6\text{B}_{30}^{2-}$ (DA-2) in the temperature range between $T = 0$ –400 K. Both the perfect endohedral metallo-borosphenes D_{3h} $\text{La}@[La_5\&B_{30}]$ (1) and D_{3h} $\text{La}@[La_5\&B_{30}]^{2-}$ (3) and slightly distorted C_s $\text{La}@[La_5\&B_{30}]^-$ (2) are composed of three inverse sandwiches $\text{La}(\eta^8\text{-B}_8)\text{La}$ on the waist and two inverse sandwiches $\text{La}(\eta^9\text{-B}_9)\text{La}$ on the top and bottom which share one apex La atom at the center and six periphery B_2 units on the surface, forming spherical trihedral structures with three octo-coordinate La atoms and two nona-coordinate La atoms as integrated parts of the cage surface. To maximize the coordination interactions between B and La atoms in the complexes, $\text{La}@[La_5\&B_{30}]^{0/-2-}$ (1/2/3) take endohedral trihedral metallo-borosphenes structures which are totally different from that of the bowl-shaped quasi-planar C_{5v} B_{30} .⁵⁵ As detailed below in bonding analyses, the central La atoms play an essential role in stabilizing these La-centered trihedral spherical species. It participates in twenty-five delocalized coordination bonds involving all the thirty B atoms as ligands on the boron framework and five La atoms as coordination centers on the cage surface.

Detailed BOMD simulations indicate that both the high-symmetry D_{3h} $\text{La}@[La_5\&B_{30}]$ (1) and D_{3h} $\text{La}@[La_5\&B_{30}]^{2-}$ (3) are dynamically stable, with the small calculated root-mean-square-deviations of RMSD = 0.13, 0.14 Å and maximum bond length deviations of MAXD = 0.45, 0.44 Å at 1000 K, respectively (Fig. S8 and S9, ESI†). The six La atoms in D_{3h} $\text{La}@[La_5\&B_{30}]^{0/2-}$ (1/3) can be classified into three categories, including one La atom at the center (La_c), three equivalent octo-coordinate La atoms on the waist (La_w), and two equivalent nona-coordinate La atoms at the opposite ends of the elongated sphere (La_e), with the optimized La-La distances of $r(\text{La}_c\text{-La}_e) = 3.53/3.51$ Å and $r(\text{La}_c\text{-La}_w) = 3.78/3.74$ Å. Detailed NBO analyses indicate that La_c , La_w , and La_e in $\text{La}@[La_5\&B_{30}]$ (1) possess the natural net atomic charges of $q_{\text{La}} = +0.84$, $+1.74$, and $+1.75$ $|e|$, total Wiberg bond orders of $\text{WBI}_{\text{La}} = 4.26$, 2.56, and 2.55, and electronic configurations of $[\text{Xe}]5d^{1.18}6s^{0.19}6p^{0.54}6d^{0.29}$, $[\text{Xe}]5d^{1.22}6s^{0.07}6p^{0.07}6d^{0.02}$, and $[\text{Xe}]5d^{1.19}6s^{0.07}6p^{0.09}6d^{0.04}$, respectively, indicating that the six La atoms donate their 6s electrons almost completely to the B_{30} ligand to form effective La-B coordination interactions. The especially higher total bond order ($\text{WBI}_{\text{La}} = 4.26$) and lower atomic charge ($q_{\text{La}} = +0.84$ $|e|$) of the central La atom clearly demonstrate the unique role it plays in stabilizing the La-centered metallo-borosphenes. The calculated La-La bond orders of

$\text{WBI}(\text{La}_c\text{-La}_e) = 0.26$ and $\text{WBI}(\text{La}_c\text{-La}_w) = 0.15$ indicate that the central La forms stronger La-La covalent bonding in vertical direction than in horizontal direction. The thirty B atoms in the B_{30} framework in $\text{La}@[La_5\&B_{30}]$ (1) carry the average negative atomic charge of $q_{\text{B}} = -0.32$ $|e|$, indicating effective La-6s \rightarrow B-2p charge-transfer from the La coordination centers to B_{30} ligand in the complex.

Using D_{3h} $\text{La}@[La_5\&B_{30}]$ (1) as building blocks, the 1D nanowire La_4B_{21} (4, $P31m$) can be constructed as an extension of the system along the C_3 axis. La_4B_{21} (4) contains a La-La string inside a $\text{La}_3\&\text{B}_{21}$ nanotube ($P62m$) with the elongated La-La distance of $r_{\text{La-La}} = 4.437$ Å. A detailed *ab initio* molecular dynamic (AIMD) simulation with a 1×3 supercell exhibits no obvious structural distortion or bond breakage in La_4B_{21} (4) in 10 ps at 500 K, suggesting that La_4B_{21} (4) is thermodynamically stable at high temperatures. The calculated phonon dispersion curves with a 1×2 supercell also indicate that La_4B_{21} (4) is dynamically stable with a negligible imaginary frequency of -11.3 cm^{-1} (Fig. S10, ESI†). The calculated band structures and projected densities of states (PDOS) of La_4B_{21} (4) depicted in Fig. S11 (ESI†) clearly demonstrate that 1D nanowire is metallic in nature. Both the B-2p orbitals and the La-5d orbitals contribute to the calculated densities of states near the Fermi level. Detailed Bader charge analyses indicate that the central La atom and the surface La atoms in La_4B_{21} (4) carry the positive atomic charges of $q_{\text{La}} = +1.55$ $|e|$ and $+1.43$ $|e|$, respectively, with the surface B atoms possessing the average atomic charge of $q_{\text{B}} = -0.28$ $|e|$, overall similar to the charge distribution in $\text{La}@[La_5\&B_{30}]$ (1). We notice that the central La atom in 1D La_4B_{21} (4) is slightly off-centered in the unit cell, with the elongated La-La distances of $r_{\text{La-La}} = 4.437$ Å along the C_3 axis which effectively weaken the La-La interaction along the encapsulated La-La string.

Chemical bonding analyses

The high stabilities of these endohedral metallo-borosphenes originate from their unique electronic configurations and bonding patterns. We choose to analyse the AdNDP bonding pattern of the singlet $\text{La}@[La_5\&B_{30}]^{2-}$ (3) in Fig. 2 to reveal both the localized and delocalized bonds it possesses. The dianion possesses 12 2c-2e B-B σ bonds and 18 3c-2e σ bonds evenly distributed on the B_{30} framework in the first row in the overall symmetry of D_{3h} . The remaining 25 bonds are delocalized over three $\text{La}(\eta^8\text{-B}_8)\text{La}$ inverse sandwiches on the waist and two $\text{La}(\eta^9\text{-B}_9)\text{La}$ inverse sandwiches on the top and bottom, including 3 10c-2e $\text{B}_8(\sigma)\text{-La}_2(d_{\sigma/\pi})$ bonds, 1 10c-2e π bond, and 1 10c-2e $\text{B}_8(\pi)\text{-La}_2(d_\delta)$ bond over each $\text{La}(\eta^8\text{-B}_8)\text{La}$ inverse sandwich subunit in the second row and 3 11c-2e $\text{B}_9(\sigma)\text{-La}_2(d_{\sigma/\pi})$ bonds and 2 11c-2e $\text{B}_9(\pi)\text{-La}_2(d_\delta)$ bonds over each $\text{La}(\eta^9\text{-B}_9)\text{La}$ inverse sandwich in the third row. There exist thus three delocalized σ bonds matching the $4n + 2$ aromatic rule ($n = 1$) over each inverse sandwich on the cage surface, rendering local σ aromaticity to each inverse sandwich subunit in the system. Overall, the closed-shell $\text{La}@[La_5\&B_{30}]^{2-}$ (3) possesses 25 delocalized bonds (50 electrons) over the cage surface and follows the Hirsch rule⁵⁶ of electron count $2(N + 1)^2$ with $N = 4$ for

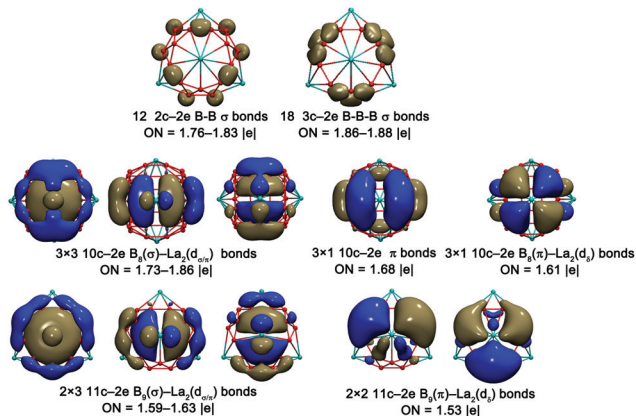


Fig. 2 AdNDP bonding patterns of D_{3h} $\text{La}@[La_5B_{30}]^{2-}$ (3), with occupation numbers (ONs) indicated.

spherical aromaticity, while $\text{La}@[La_5B_{30}]$ (1) with two less valence electrons than $\text{La}@[La_5B_{30}]^{2-}$ (3) matches the $2(N+1)^2 - 2$ requirement for spherical aromaticity in triplet systems with two unpaired electrons ($N = 4$). Such unique bonding patterns render high stabilities to these endohedral spherical species.

The spherical aromaticities of the closed-shell $\text{La}@[La_5B_{30}]$ (1) and D_{3h} $\text{La}@[La_5B_{30}]^{2-}$ (3) are further demonstrated by their iso-chemical shielding surfaces (ICSSs) based on the calculated NICS-ZZ components, as shown in Fig. 3(a and b), respectively, where the z axis is parallel to the C_3 molecular axis of the system. It can be clearly seen that the space inside the $\text{La}@[La_5B_{30}]^{0/2-}$ (1/3) spherical trihedrons or within about 1.0 Å above the La atom on the top in vertical direction belong to chemical shielding regions with negative NICS-ZZ values (highlighted in yellow), while the belt-like chemical de-shielding regions are located around the waist in horizontal direction with positive NICS-ZZ values (highlighted in green). Such ICSS surfaces appear to be similar to that of the prototypical

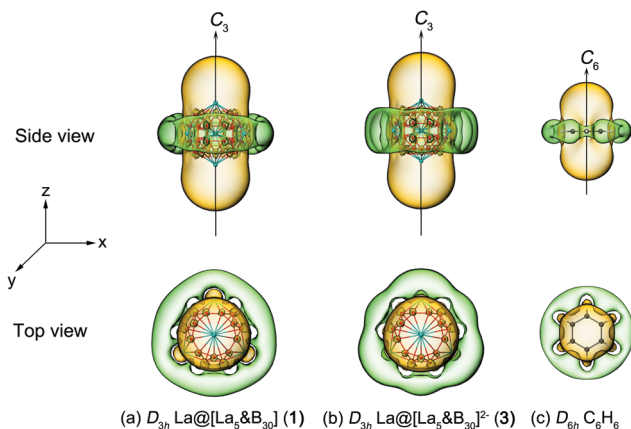


Fig. 3 Side and top views of the iso-chemical shielding surfaces (ICSSs) of (a) $\text{La}@[La_5B_{30}]$ (1), and (b) $\text{La}@[La_5B_{30}]^{2-}$ (3) based on their calculated NICS-ZZ components, compared with that of (c) benzene C_6H_6 , with the main molecular axes designated as the z axis in the vertical direction. Yellow and green regions stand for chemical shielding and de-shielding areas, respectively.

aromatic benzene C_6H_6 (Fig. 3(d)), well supporting the aromatic nature of both $\text{La}@[La_5B_{30}]$ (1) and $\text{La}@[La_5B_{30}]^{2-}$ (3) discussed above. Similar ICSS surfaces (Fig. S12, ESI[†]) exist for open-shell C_s $\text{La}@[La_5B_{30}]^-$ (2), unveiling the spherical aromatic nature of the monoanion.

Simulated IR, Raman and PE spectra

Infrared (IR) spectra and PE spectroscopy have proven to be powerful techniques in characterizing novel gas-phase clusters. The simulated the IR and Raman spectra of $\text{La}@[La_5B_{30}]$ (1) at PBE0 level are depicted in Fig. 4(a and b), respectively. The four major IR peaks of the neutral occur at 249 (a_2''), 278 (e'), 533 (e'), and 937 (a_2'') cm^{-1} , respectively, corresponding mainly to the vibrations of the B_{30} boron skeleton. The three strong Raman peaks occur at 144 (a_1'), 172 (a_1'), and 1110 (e') cm^{-1} , with the first two corresponding to typical “radial breathing modes” (RBMs) of the endohedral structure which can be used to characterize hollow boron nanostructures in experiments. The simulated PE spectrum of $\text{La}@[La_5B_{30}]^-$ (2) at TD-DFT-PBE0 with 400 excited triplet states and 400 excited singlet states considered is depicted in Fig. 4(c). Since $\text{La}_6B_{30}^-$ has a

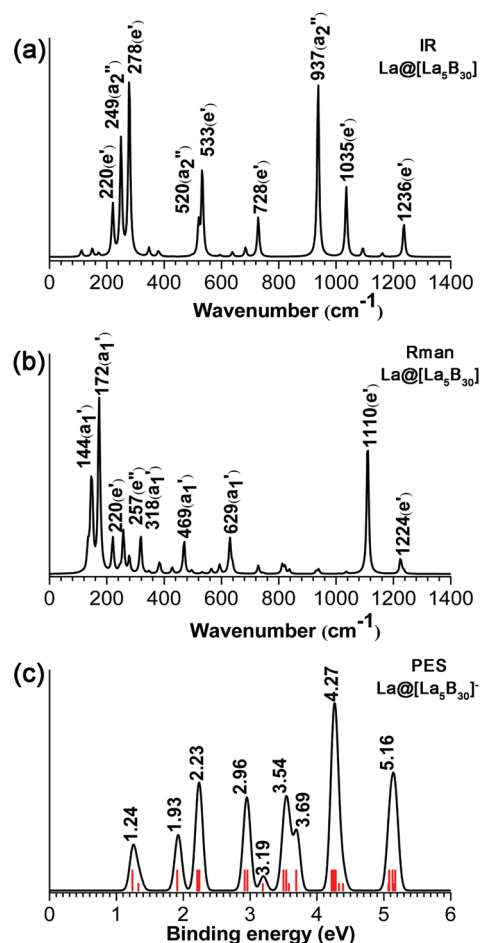


Fig. 4 Simulated (a) IR and (b) Raman spectra of D_{3h} $\text{La}@[La_5B_{30}]$ (1) and (c) PE spectroscopy of C_s $\text{La}@[La_5B_{30}]^-$ (3) and at PBE0 level. In (c), the longer red bars represent triplet excitations while the shorter ones stand for singlet excitations.

doublet state, one-electron detachment from the anion could lead to singlet or triplet final states in the neutral. The first vertical detachment energy (VDE) at 1.24 eV for $\text{La}@\text{[La}_5\&\text{B}_{30}]^-$ (C_s , $^2A'$) was calculated as the energy difference between the anionic ground state and the neutral ground state at the optimized anion geometry. Higher binding energy VDEs were calculated using the time-dependent DFT method (TD-DFT) at PBE0/6-311+G(d) level which correspond to detachment transitions to the excited states of the neutral. $\text{La}@\text{[La}_5\&\text{B}_{30}]^-$ possesses seven well-separated vertical detachment energies centered at VDE = 1.24, 1.93, 2.23, 2.96, 3.54, 4.27 and 5.16 eV, respectively. The first adiabatic detachment energy calculated at ADE = 1.21 eV represents the electron affinity (EA) of neutral D_{3h} $\text{La}@\text{[La}_5\&\text{B}_{30}]$ (1).

Conclusions

Based on extensive GM searches and first-principles theoretical calculations, we have predicted in this work the GM structures of endohedral metallo-borospherenes D_{3h} $\text{La}@\text{[La}_5\&\text{B}_{30}]$ (1), C_s $\text{La}@\text{[La}_5\&\text{B}_{30}]^-$ (2), and D_{3h} $\text{La}@\text{[La}_5\&\text{B}_{30}]^{2-}$ (3) which possess typical spherical aromaticity. These metallo-borospherenes are stacks of three inverse sandwich $\text{La}(\eta^8\text{-B}_8)\text{La}$ and two inverse sandwich $\text{La}(\eta^9\text{-B}_9)\text{La}$ which share one apex La atom at the center and six periphery B_2 units on the cage surface, while the 1D nanowire La_4B_{21} (4, $P31m$) as an extension of $\text{La}@\text{[La}_5\&\text{B}_{30}]$ (1) appears to be metallic in nature. We have also simulated the IR and Raman spectra of $\text{La}@\text{[La}_5\&\text{B}_{30}]$ (1) and PE spectra of its monoanion C_s $\text{La}@\text{[La}_5\&\text{B}_{30}]^-$ (2) to facilitate their characterizations in gas-phase experiments. Medium-sized metal-doped boron nanoclusters and their low-dimensional nanomaterials with interesting geometrical and electronic structures as possible electronic nanodevices remain a fertile area to be explored in both experiments and theory.

Conflicts of interest

There are no conflicts to declare.

Acknowledgements

The work was supported by the National Natural Science Foundation of China (21720102006 and 21973057 to S.-D. Li).

Notes and references

- F. A. Cotton, G. Wilkinson, C. A. Murillo and M. Bochmann, *Advanced Inorganic Chemistry*, Wiley, New York, 6th edn, 1999.
- L. S. Wang, *Int. Rev. Phys. Chem.*, 2016, **35**, 69.
- T. Jian, X. N. Chen, S. D. Li, A. I. Boldyrev, J. Li and L. S. Wang, *Chem. Soc. Rev.*, 2019, **48**, 3550.
- L. S. Wang, *Int. Rev. Phys. Chem.*, 2016, **35**, 69.
- Y. J. Wang, Y. F. Zhao, W. L. Li, T. Jian, Q. Chen, X. R. You, T. Ou, X. Y. Zhao, H. J. Zhai, S. D. Li, J. Li and L. S. Wang, *J. Chem. Phys.*, 2016, **144**, 064307.
- Q. Chen, W. L. Li, Y. F. Zhao, S. Y. Zhang, H. S. Hu, H. Bai, H. R. Li, W. J. Tian, H. G. Lu, H. J. Zhai, S. D. Li, J. Li and L. S. Wang, *ACS Nano*, 2015, **9**, 754.
- H. J. Zhai, Y. F. Zhao, W. L. Li, Q. Chen, H. Bai, H. S. Hu, Z. A. Piazza, W. J. Tian, H. G. Lu, Y. B. Wu, Y. W. Mu, G. F. Wei, Z. P. Liu, J. Li, S. D. Li and L. S. Wang, *Nat. Chem.*, 2014, **6**, 727.
- W. J. Chen, Y. Y. Ma, T. T. Chen, M. Z. Ao, D. F. Yuan, Q. Chen, X. X. Tian, Y. W. Mu, S. D. Li and L. S. Wang, *Nanoscale*, 2021, **13**, 3868.
- L. Pei, Q. Q. Yan and S. D. Li, *Eur. J. Inorg. Chem.*, 2021, 2618.
- L. Pei, Y. Y. Ma, M. Yan, M. Zhang, R. N. Yuan, Q. Chen, W. Y. Zan, Y. W. Mu and S. D. Li, *Eur. J. Inorg. Chem.*, 2020, 3296.
- Q. Q. Yan, L. Pei and S. D. Li, *J. Mol. Model.*, 2021, **27**, 364.
- E. Oger, N. R. M. Crawford, R. Kelting, P. Weis, M. M. Kappes and R. Ahlrichs, *Angew. Chem., Int. Ed.*, 2007, **46**, 8503.
- N. G. Szwacki, A. Sadrzadeh and B. I. Yakobson, *Phys. Rev. Lett.*, 2007, **98**, 166804.
- A. Sadrzadeh, O. V. Pupyshva, A. K. Singh and B. I. Yakobson, *J. Phys. Chem. A*, 2008, **112**, 13679.
- J. J. Zhao, L. Wang, F. Y. Li and Z. F. Chen, *J. Phys. Chem. A*, 2010, **114**, 9969.
- T. R. Galeev, C. Romanescu, W. L. Li, L. S. Wang and A. I. Boldyrev, *Angew. Chem., Int. Ed.*, 2012, **51**, 2101.
- I. A. Popov, T. Jian, G. V. Lopez, A. I. Boldyrev and L. S. Wang, *Nat. Commun.*, 2015, **6**, 8654.
- T. T. Chen, W. L. Li, J. Li and L. S. Wang, *Chem. Sci.*, 2019, **10**, 2534.
- W. L. Li, T. T. Chen, D. H. Xing, X. Chen, J. Li and L. S. Wang, *Proc. Natl. Acad. Sci. U. S. A.*, 2018, **115**, E6972.
- T. T. Chen, W. L. Li, W. J. Chen, J. Li and L. S. Wang, *Chem. Commun.*, 2019, **55**, 7864.
- T. T. Chen, W. L. Li, W. J. Chen, X. H. Yu, X. R. Dong, J. Li and L. S. Wang, *Nat. Commun.*, 2020, **11**, 2766.
- X. Y. Zhao, M. Yan, Z. H. Wei and S. D. Li, *RSC Adv.*, 2020, **10**, 34225.
- Y. Zhang, X. Y. Zhao, M. Yan and S. D. Li, *RSC Adv.*, 2020, **10**, 29320.
- Y. Zhang, X. Q. Lu, M. Yan and S. D. Li, *ACS Omega*, 2021, **6**, 10991.
- H. R. Li, H. Liu, X. X. Tian, W. Y. Zan, Y. W. Mu, H. G. Lu, J. Li, Y. K. Wang and S. D. Li, *Phys. Chem. Chem. Phys.*, 2017, **19**, 27025.
- J. P. Dognon, C. Clavaguéra and P. Pykkö, *J. Am. Chem. Soc.*, 2009, **131**, 238.
- X. Q. Lu, M. Z. Ao, X. X. Tian, W. Y. Zan, Y. W. Mu and S. D. Li, *RSC Adv.*, 2020, **10**, 12469.
- X. Chen, Y. F. Zhao, Y. Y. Zhang and J. Li, *J. Comput. Chem.*, 2019, **40**, 1105.
- Y. Zhao, X. Chen and J. Li, *Nano Res.*, 2017, **10**, 3407.
- C. Adamo and V. Barone, *J. Chem. Phys.*, 1999, **110**, 6158.

- 31 V. N. Staroverov, G. E. Scuseria, J. M. Tao and J. P. Perdew, *J. Chem. Phys.*, 2003, **119**, 12129.
- 32 R. Krishnan, J. S. Binkley, R. Seeger and J. A. Pople, *J. Chem. Phys.*, 1980, **72**, 650.
- 33 M. Dolg, H. Stoll, A. Savin and H. Preuss, *Theor. Chim. Acta*, 1989, **75**, 173.
- 34 M. Dolg, H. Stoll and H. Preuss, *Theor. Chim. Acta*, 1993, **85**, 441.
- 35 M. J. Frisch, *et al.*, *Gaussian 09, Revision D.01*, Gaussian Inc., Wallingford, CT, 2009.
- 36 G. D. Purvis III and R. J. Bartlett, *J. Chem. Phys.*, 1982, **76**, 1910.
- 37 K. Raghavachari, G. W. Trucks, J. A. Pople and M. Head-Gordon, *Chem. Phys. Lett.*, 1989, **157**, 479.
- 38 H. J. Werner, P. J. Knowles, G. Knizia, F. R. Manby and M. Schütz, *WIREs Comput. Mol. Sci.*, 2012, **2**, 242.
- 39 P. E. D. Glendening, J. K. Badenhop, A. E. Reed, J. E. Carpenter, J. A. Bohmann, C. M. Morales, C. R. Landis and F. Weinhold, *NBO 6.0*, 2013.
- 40 D. Y. Zubarev and A. I. Boldyrev, *Phys. Chem. Chem. Phys.*, 2008, **10**, 5207.
- 41 N. V. Tkachenko and A. I. Boldyrev, *Phys. Chem. Chem. Phys.*, 2019, **21**, 9590.
- 42 J. V. Vondele, M. Krack, F. Mohamed, M. Parrinello, T. Chassaing and J. Hutter, *Comput. Phys. Commun.*, 2005, **167**, 103.
- 43 T. Lu and F. Chen, *J. Comput. Chem.*, 2012, **33**, 580.
- 44 W. Humphrey, A. Dalke and K. Schulten, *J. Mol. Graphics*, 1996, **14**, 33.
- 45 R. Bauernschmitt and R. Ahlrichs, *Chem. Phys. Lett.*, 1996, **256**, 454.
- 46 G. Kresse and J. Furthmüller, *Comput. Mater. Sci.*, 1996, **6**, 15.
- 47 G. Kresse and J. Furthmüller, *Phys. Rev. B: Condens. Matter Mater. Phys.*, 1996, **54**, 11169.
- 48 P. E. Blöchl, *Phys. Rev. B: Condens. Matter Mater. Phys.*, 1994, **50**, 17953.
- 49 G. Kresse and D. Joubert, *Phys. Rev. B: Condens. Matter Mater. Phys.*, 1999, **59**, 1758.
- 50 J. P. Perdew, K. Burke and M. Ernzerhof, *Phys. Rev. Lett.*, 1996, **77**, 3865.
- 51 J. P. Perdew, K. Burke and M. Ernzerhof, *Phys. Rev. Lett.*, 1997, **78**, 1396.
- 52 I. V. Solov'yev and P. H. Dederichs, *Phys. Rev. B: Condens. Matter Mater. Phys.*, 1994, **50**, 16861.
- 53 V. I. Anisimov, J. Zaanen and O. K. Andersen, *Phys. Rev. B: Condens. Matter Mater. Phys.*, 1991, **44**, 943.
- 54 A. Togo, F. Oba and I. Tanaka, *Phys. Rev. B: Condens. Matter Mater. Phys.*, 2008, **78**, 134106.
- 55 T. B. Tai, L. V. Duong, H. T. Pham, D. T. T. Maia and M. T. Nguyen, *Chem. Commun.*, 2014, **50**, 1558.
- 56 A. Hirsch, Z. Chen and H. Jiao, *Angew. Chem.*, 2000, **39**, 3915.